A molecular insight into the nature of crystallographic mismatches in self-assembled fibrillar networks under non-isothermal crystallization conditions

Ricky Lam,[a] Luca Quaroni,[bc] Tor Pederson[b] and Michael A. Rogers*[a]

Received 18th September 2009, Accepted 29th October 2009
First published as an Advance Article on the web 13th November 2009
DOI: 10.1039/b919477k

The lengths of the 12-hydroxystearic acid (12HSA) fibers are influenced by crystallographic mismatches resulting from the incorporation of 12HSA monomers into the crystal lattice in an imperfect manner. On a molecular level, this can be differentiated using synchrotron Fourier transform infrared (FTIR) spectroscopy by monitoring the change in area of the 1700 cm^{-1} and 3200 cm^{-1} peaks, corresponding, respectively, to the dimerization of the carboxylic acid groups and hydroxyl non-covalent interactions, during crystallization. The crystallographic mismatch is attributed to a plateau in the apparent rate constant for the dimerization of the carboxylic acid head groups while the hydroxyl interactions linearly increase as a function of cooling rate (ϕ). The rate constant for hydroxyl interactions linearly increases as a function of cooling rate while a plateau is observed for the rate of dimerization at cooling rates between 5 and 7 °C min^{-1}. At cooling rates greater than 5 to 7 °C min^{-1} 12HSA monomers do not effectively dimerize before being incorporated into the crystal lattice causing crystal imperfections impeding linear epitaxial crystal growth and produces branched fibers. At slow cooling rates (*i.e.*, less than 5 to 7 °C min^{-1}), long fibers are produced with a fractal dimension between 0.95 and 1.05 and for rapid cooling rates (*i.e.*, greater than 5 to 7 °C min^{-1}) short branched fibers are produced with a fractal dimension between 1.15 and 1.32.

Introduction

Fundamental research on molecular gels, capable of self-assembling into fibrillar networks, has primarily focused on structural and mechanical characterization of these soft materials.[1] This, in part, is due to the numerous, assorted applications of these complex systems including: drug delivery,[2,3] tissue engineering,[4] lipid structuring[5–7] and scaffolding systems.[8] To illustrate the structural significance of these materials in practical applications, such as drug delivery, the rate of release is a function of the bioseparation process. This separation process is directly related to the mesh size distribution of the network.[9,10] Therefore, the ability to manipulate and control the rheological network properties of the desired gelator–solvent combinations is crucial in achieving the desired physical properties of these soft materials. Due to the importance of the rheological and network properties, the degree of branching and hence the mesh size distribution have been extensively examined under isothermal[11–14] and non-isothermal conditions.[15,16] The diversity of the microscopic and mesoscopic structures of low molecular weight organogels makes them interesting soft materials with numerous theoretical and practical applications.[17]

Thermoreversible molecular gels are capable of aggregating upon cooling the organogelator–solvent melt below the gelators' melting point leading to the formation of a supersaturated state.[18] The supersaturated state (also termed supercooling or undercooling) is achieved *via* isothermal or non-isothermal cooling conditions. Supercooling (τ) has been defined under isothermal conditions as $\tau = (T^* - T)/T^*$ where T^* is the equilibrium temperature and T is the temperature of gelation.[14] While for non-isothermal conditions the comparable supercooling-time exposure (β) term is defined as $\beta = \frac{1}{2}(\Delta T_c)^2/\phi$ where ΔT_c is equal to $T_m - T_c$ and T_m is the melting temperature, T_c is the crystallization temperature and ϕ is the cooling rate.[15,16] Cooling beyond the formation of the supersaturated state causes the gelator molecules to microscopically phase separate and self-assemble *via* stochastic nucleation events driven by enthalpic forces.[18] Following nucleation, crystal growth causes gelator molecules to aggregate into a network of forming rods, tubes, or sheets *via* non-covalent interactions. The aggregation process requires a meticulous balance between the contrasting parameters of solubility and those controlling epitaxial growth.[19] Molecular gels contain fibers that form a 3-dimensional network interacting *via* transient and permanent junction zones.[20] Permanent junction zones are effective at entraining the liquid apolar phase in the mesh-like network arising because of crystallographic mismatches at the interface of the growing one-dimensional crystals, resulting in branch points and truncations along the fiber.[20,21]

Recent work by Liu has advanced the understanding on how these fibers can be engineered *via* the modification of the isothermal crystallization conditions of the gelator–solvent system.[14] Liu has been instrumental in developing the theory on crystallographic mismatches used to model the branching and generation of permanent junction zones. Significant evidence has been provided to support the nucleation–growth–crystallographic mismatch branching (CMB) mechanism (Fig. 1).

[a]*Department of Food and Bioproduct Sciences, University of Saskatchewan, Saskatoon, SK, Canada S7N 5A8. E-mail: Michael.rogers@usask.ca; Fax: +1 306 966 8898; Tel: +1 306 966 5028*
[b]*Canadian Light Source, Saskatoon, SK, Canada S7N 0X4*
[c]*Department of Chemistry, University of Manitoba, Winnipeg, MN, Canada R3T 2N2*

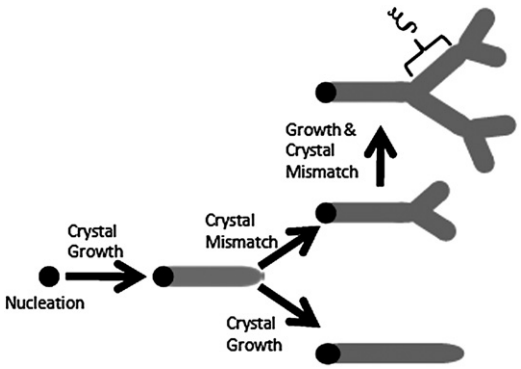

Fig. 1 Nucleation and crystal growth mechanism using the crystallographic mismatch theory (adapted from ref. 14).

The CMB method suggests that with low degrees of undercooling, following nucleation, the fibers grow one-dimensionally with little branching, interpenetration and entanglement.[20] At low degrees of bulk supersaturation, the crystallographic mismatch nucleation barrier (ΔG^*) is very high, favoring one-dimensional fiber growth with a corresponding large correlation length (ξ).[20] However, when the crystallization temperature is decreased an increase in the supersaturation causes the crystallographic mismatch barrier to be significantly reduced increasing the fiber tip branching.[20] The highly branched fibers (*i.e.*, short correlation length (ξ)) coincide with smaller pore sizes.[20] Recently, it has been shown that increased supercooling leads to more elastic gels due to the shorter branched fibers.[9,14] However, at this time, molecular evidence has not been provided to support or reject the theory of crystallographic mismatches and it is our aim to examine the crystallographic mismatch theory by examining the non-covalent interactions which allow the gelator molecules to assemble into fibrillar aggregates.

Methods

Sample preparation

DL-12-Hydroxystearic acid was obtained from Nu-check Prep (Elysian, MN, USA) and heavy mineral oil was obtained from Sigma-Aldrich (Oakville, ON, CAN) and were used as received. 2.5 wt% samples of 12HSA in mineral oil were prepared in triplicate by heating the 12HSA in heavy mineral oil to 90 °C for 30 min and were stored at room temperature.

Polarized light microscopy

Polarized light micrographs were acquired using a Nikon Eclipse E400 light microscope equipped with a Nikon DS-FiL color camera and a long working distance 10× lens and condenser with a resolution of 2560 by 1920. Non-isothermal cooling conditions from 1 °C min^{-1} to 20 °C min^{-1} were carried out using a temperature controlled stage (LTS120 and PE94 temperature controller (Linkam, Surrey, UK)). Images were acquired when the system reached 30 °C. Fiber length was measured using the software Image J (Bethesda, Maryland, USA) where the number of pixels along a fiber was determined and calibrated to a 100 μm magnification bar imaged under the same conditions as the gels.

Small deformation rheology

An AR 1000 rheometer (TA instruments, New Castle, DE) was used to probe the macroscopic properties of the materials during the formation of the network. A 4 cm flat steel parallel plate (TA Instruments, New Castle, DE) and a gap of 1000 μm were used to carry out the oscillatory measurements during crystallization. Small deformation oscillatory rheology was employed to monitor the evolution of the modulus (G^*) as a function of time during controlled cooling rates at 1 Hz and 10 Pa. 10 Pa was chosen as the controlled stress because it is the lowest value obtained in the linear viscoelastic region (LVR).

Synchrotron Fourier transform infrared spectroscopy

A drop of sample was placed between two CaF_2 optical windows (25 mm diameter, 2 mm thick) separated with a 15 μm Teflon spacer. The samples were then cooled on a Linkam LTS120 controlled temperature stage (Linkam, Surrey, UK) with cooling rates between 1 °C min^{-1} and 20 °C min^{-1}. Fourier transform infrared (FTIR) spectra were collected using the end station of the mid-IR beamline (beamline 01B1-01, Canadian Light Source, Saskatoon, SK). The end station is comprised of a Bruker Optics IFS66v/S interferometer coupled to a Hyperion 2000 IR microscope (Bruker Optics, Billerica, MA, USA). Light is focused on the sample using a 15× magnification Schwarzschild condenser, collected by a 15× magnification Schwarzschild objective with the aperture set to a spot size of 40 μm by 40 μm and detected by a liquid nitrogen cooled narrowband MCT detector utilizing a 100 μm sensing element.

A KBr-supported Ge multilayer beamsplitter was used to measure spectra in the mid-infrared spectral region. Measurements were performed using OPUS 6.5 software (Bruker Optics, Billerica, MA). The measured interferograms were an average of 32 scans and were recorded by scanning the moving mirror at 40 kHz (in relation to the reference HeNe laser wavelength of 632.8 nm). The wavelength range collected was 690 to 7899 cm^{-1} with a spectral resolution of 4 cm^{-1}. Single channel traces were obtained using the fast Fourier transform algorithm, without any zero-filling, after applying a Blackman–Harris 3-Term apodization function. For single spectra, measurements' reference single channel traces were carried out in the molten state.

Results and discussions

Fig. 2 illustrates images of 2.5 wt% 12-hydroxystearic acid (12HSA) in mineral oil which produces a transparent gel when cooled below the melting point of the gelator. Fig. 2A and B represent cooling rates of 1 and 4 °C min^{-1} which are subjected to a lesser degree of supercooling, Fig. 2C and D represent cooling rates of 7 and 20 °C min^{-1}. The faster cooling rates (Fig. 2C and D) produced shorter fibers due to the presence of crystallographic mismatches. This corresponds well to results observed by Liu *et al.*,[21] where they observed the formation of highly branched networks when isothermally cooled to 20 °C, while little branching was observed when isothermally cooled to 50 and 55 °C. In their system, they found that the correlation length (ξ) linearly decreased as a function of supercooling ($(T^* - T)/T^*$) until reaching a plateau where the fiber no longer decreases in length (ξ).[14] Under non-isothermal conditions the lengths of the

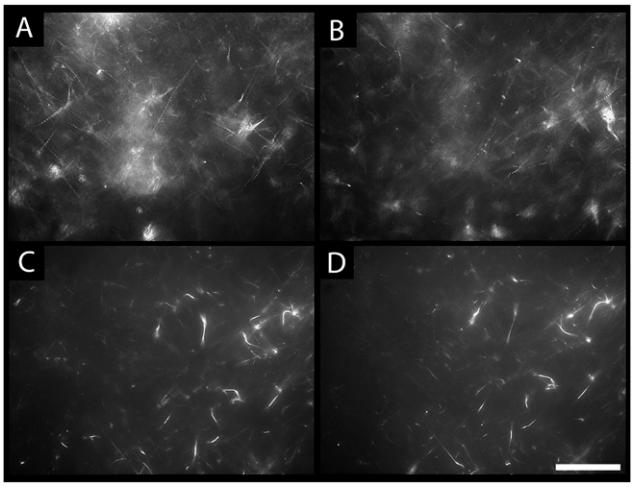

Fig. 2 2.5 wt% 12HSA in mineral oil organogels at 30 °C cooled at 1 °C min^{-1} (A), 4 °C min^{-1} (B), 7 °C min^{-1} (C) and 20 °C min^{-1} (D). Magnification bar = 100 μm.

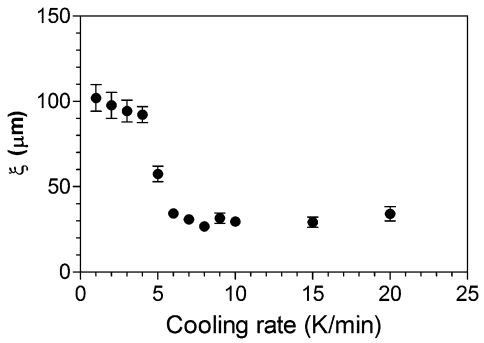

Fig. 3 Correlation length of 2.5 wt% 12HSA fibers in mineral oil measured from the micrographs obtained at 30 °C after they had been cooled from 90 °C at varying cooling rates.

fibers uninterrupted by crystallographic mismatches were measured (Fig. 3). A similar trend was observed where the correlation length decreased linearly as a function of cooling rate between 1 °C min^{-1} and 4 °C min^{-1}. Cooling rates greater than 4 °C min^{-1} resulted in an abrupt change in the fiber length resulting in significantly ($p < 0.05$) shorter fibers. Previously, using a modified Avrami equation for non-isothermal cooling conditions we illustrated that the length of fibers and rate of fiber growth have two linear regimes where the distinction is at approximately 5–7 °C min^{-1}.[15,16] It has been established that molecular self-assembly occurs *via* highly specific non-covalent interactions occurring *via* Liu's nucleation–growth–crystallographic mismatch–growth mechanism.[14]

Typically crystal growth is thought of in integer values where fibers would be 1-dimensional, platelets would be 2-dimensional and spherulites would correspond to 3-dimensional growth. However, in many instances materials grow in a fractal or self-similar nature regardless of the length scale examined.[12] Liu and Sawant[12] have developed a fractal rheological method for quantifying isothermal crystallization of organogels which originates from the Cayley tree network structure and the Avrami model leading to the following form:

$$\ln[1 - X_{cr}] = -k^{o}\left(t - t_{g}\right)^{D_f} \quad (1)$$

where:

$$X_{cr}(t) = \frac{G^{*}(t) - G_{0}^{*}}{G^{*}(\max) - G_{0}^{*}} \quad (2)$$

where G^* is the modulus at a given time, G_0^* is the initial modulus and G^*(max) is the maximum modulus, k^o is a constant related to the growth rate, t is the time, t_g is the gelation time and D_f is the fractal dimension.[12] Since the rheological fractal dimension is a measure of the solid network structure, the spatial distribution of the solid phase, the degree of branching and fiber–fiber interactions and not solely a measure of a solid phase volume, the assumptions which apply to the Avrami model do not hold. However, the fractal form is consistent with numerous other researchers and the exponent D_f derived from Liu's model is a function of the network structure. However, the fractal value is theoretically different from the exponent (n) in the Avrami model which only is correct if the physical attribute being measured is a function of the solid phase volume. D_f represents the dimensionality of crystal network growth while n from the Avrami model incorporates not only the dimensionality of crystal growth but also the mode of nucleation.

Rheological data were collected (Fig. 4A and B) and transformed using these equations to calculate the fractal dimension for 12HSA under different non-isothermal conditions (Fig. 4C and D). It was observed that the fibers which developed under slow cooling rates had longer correlation length (Fig. 3) and similar fractal values (Table 1). For long one-dimensional fibers (*i.e.*, cooling rates less than 4 °C min^{-1}) the corresponding fractal values were of between 0.95 and 1.08 indicating "fiber-like" growth. At accelerated cooling rates (*i.e.*, cooling rates greater than 5 °C min^{-1}) there is an increase in the fractal value between 1.15 and 1.32. This would indicate that the fibers are becoming less linear and coincide with a greater degree of branching. Using both the correlation length determined *via* microscopy (Fig. 3) and the fractal dimension determined by rheology (Fig. 4 and Table 1) it is obvious that cooling rates greater than 5 °C min^{-1} result in crystallographic mismatches. Therefore, it is assured that these branch points are a result of a crystallographic mismatch or

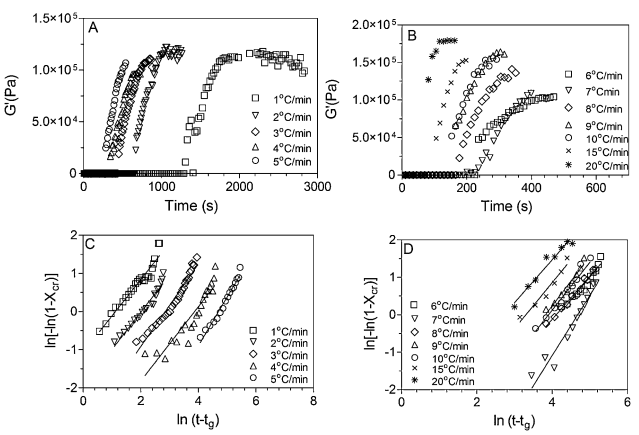

Fig. 4 The evolution of G^* as a function of time during gelation under non-isothermal conditions for slow cooling rates (A) and fast cooling rates (B). The dependence of $\ln[-\ln(1 - X_{cr})]$ on $\ln(t - t_g)$ to determine the fractal values under different non-isothermal cooling profiles (C and D). Data were shifted to prevent overlap (C).

Table 1 Dependence of the average fractal dimension and the standard deviation calculated using non-isothermal cooling rates determined using small deformation rheology

Cooling rate/°C min^{-1}	1	2	3	4	5	6	7	8	9	10	15	20
D_f	0.95 ± 0.05	0.98 ± 0.05	1.08 ± 0.04	0.97 ± 0.08	1.28 ± 0.06	1.22 ± 0.10	1.31 ± 0.06	1.15 ± 0.05	1.32 ± 0.11	1.28 ± 0.10	1.23 ± 0.14	1.15 ± 0.10

an imperfect interaction between 12HSA molecules resulting in branched networks. Hence to observe our hypothesis that hydrogen bonding is affected during crystallographic mismatches we employed FTIR spectroscopy using synchrotron radiation.

12HSA develops fibers by two monomers dimerizing between carboxylic acid groups and longitudinal growth occurs *via* hydrogen bonding between the hydroxyl groups at carbon 12. Therefore, we can monitor these spectral features using FTIR (Fig. 5A and B). The dimerization of 12HSA may be observed *via* a shift in the spectral features due to the carboxylic acid stretch shifting from 1710 cm^{-1} to 1700 cm^{-1}.[22] During assembly of 12HSA, the spectra were recorded as a function of time for each cooling rate. As the system assembles there is a decrease in the absorbance at 1710 cm^{-1} corresponding to an increase at 1700 cm^{-1} indicating that 12HSA molecules are forming dimers. Similarly, hydrogen bonding was monitored for the hydroxyl groups which is observed as an increase in the area of the peak at position 3200 cm^{-1} (Fig. 5A and B).[22] The area under the peaks at 1700 cm^{-1} and 3200 cm^{-1} was measured and plotted as a function of time while undergoing non-isothermal cooling. To assess if any changes in the rate of evolution between these two peaks were observed the modified Avrami model was applied which has been previously reported as:[15,16]

$$Y = Y_{max}\left(1 - e^{-k_{app}(x-x_0)^n}\right) \quad (3)$$

where Y is the area under the peak at 1700 cm^{-1} or 3200 cm^{-1} (Fig. 5C and D), Y_{max} is the maximum area of peaks corresponding to hydrogen bonding between 12HSA molecules, k_{app} is the apparent rate constant for non-covalent interactions (*i.e.*, hydrogen bonding), x is the time, x_0 is the induction time and n is the dimensionality of growth. In previous work, we had confined n to be equal to two because light microscopy indicated sporadic nucleation and one-dimensional growth.[15,16] However, the Avrami model was fitted by giving an initial value of n equal to two, K and x_0 equal to zero and Y_{max} is set to the maximum absorbance observed. The graphs were fitted using Graph Pad Prism 6.0 and an iterative process (1000 iterations) was used to fit the growth curves. The coefficient of determination (R^2) for all fits was greater than 0.98. Upon fitting with the Avrami model, it was observed that regardless of the cooling rate, similar intensities of the peak area were measured meaning no significant differences were observed in the intensity of the signal (Fig. 5E). An exponential decrease in the induction time was observed as a function of cooling rate which has been previously reported (Fig. 5G).[15,16] The Avrami model suggests that for all cooling rates, the dimensionality of crystal growth is instantaneous nucleation and linear 1-dimensional growth corresponding to an Avrami exponent of $n = 1$ (Fig. 5H).[23] However, examining the apparent rate constant of hydrogen bond formation between the 12HSA carboxylic acid groups and between the hydroxyl groups we have a new insight into self-assembly and to crystallographic mismatches (Fig. 5F). It has been previously mentioned that branched fibers result from molecules being incorporated into the lattice in an imperfect manner. This would suggest that there is a significant decrease in the rate of hydrogen bonding above 5 °C min^{-1} which corresponds to the significant change in fiber length (Fig. 2). It was astounding to observe that the rate of hydroxyl hydrogen bonding changes linearly with cooling rate, and does not plateau as the cooling rate increased, which was observed by a linear increase in the rate of hydroxyl interactions. However, it was observed at cooling rates greater than

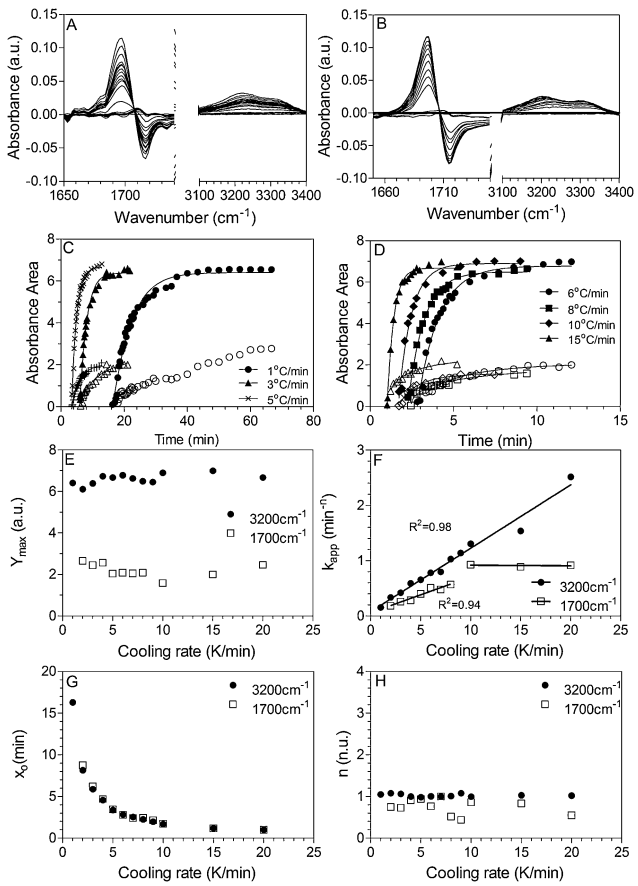

Fig. 5 Differential FTIR spectra of 12HSA assembly during slow cooling at 1° C min^{-1} collected from 90 °C to 30 °C over a 60 min period (A) and fast cooling at 10 °C min^{-1} from 90 °C to 30 °C over a 6 min period (B) non-isothermal cooling profiles. Integration of the FTIR spectra (C and D) to determine the area under the spectral features of interest (filled symbols represent absorbance at 3200 cm^{-1} and open symbols represent the absorbance at 1700 cm^{-1}). Avrami constants are determined by fitting the integrated area *versus* time to obtain maximum signal (E), apparent rate constant (F), induction time (G) and dimensionality of growth (H).

5–7 °C min^{-1} that the rate of dimerization between carboxylic acid groups plateaued (Fig. 5F). This suggests that the crystallographic mismatch for 12HSA is a result of the inability of the 12HSA monomers to effectively dimerize at rapid cooling rates. When incorporated into the crystal lattice, monomers prevent the uninterrupted longitudinal growth observed at slower cooling rates.

Conclusions

When low molecular weight organogelators self-assemble into fibrillar networks they require highly specific non-covalent interactions. Upon large degrees of supercooling, *via* isothermal or non-isothermal cooling, the fibers undergo crystallographic mismatches resulting in higher fractal networks ($D_f \approx 1.2$) affecting the hardness and the ability of the network to retain the solvent. For 12HSA, cooling rates faster than 5 °C min^{-1} result in short fibers while for slower cooling rates longer fibers result with lower fractal values ($D_f \approx 1.0$). FTIR spectroscopy revealed that nucleation for 12HSA is instantaneous while the crystallographic mismatch is a result of the rate of dimerization between carboxylic acid groups and not hydroxyl interactions.

Acknowledgements

The research described in this paper was performed at the Canadian Light Source, which is supported by NSERC, NRC, CIHR, and the University of Saskatchewan. The authors are grateful to Tim May (CLS) for beamline design, construction and for constant help in beamline upkeep. This project was supported by the National Science and Engineering Research Council of Canada (NSERC) Discovery Program.

Notes and references

1 P. Terech, *Langmuir*, 2009, **25**, 8370.
2 L. Kang, X. Y. Lu, P. D. Sawant, P. C. Ho, Y. W. Chan and S. Y. Chan, *J. Controlled Release*, 2005, **106**, 88.
3 G. Liang, Z. Yang, R. Zhang, L. Li, Y. Fan, Y. Kuang, Y. Gao, T. Wang, W. W. Lu and B. Xu, *Langmuir*, 2009, **25**, 8419.
4 X. Bu, *Langmuir*, 2009, **25**, 8375.
5 M. A. Rogers, A. J. Wright and A. G. Marangoni, *Soft Matter*, 2009, **5**, 1594.
6 A. Bot and W. G. M. Agterof, *J. Am. Oil Chem. Soc.*, 2006, **83**, 513.
7 A. Bot, R. den Adel and E. C. Roijers, *J. Am. Oil Chem. Soc.*, 2008, **85**, 1127.
8 A. Ajayaghosh, V. K. Praveen and C. Vijayakumar, *Chem. Soc. Rev.*, 2008, **37**, 109.
9 M. A. Rogers, A. J. Wright and A. G. Marangoni, *Soft Matter*, 2008, **4**, 1483.
10 J. L. Li, X. Y. Liu, R. Y. Wang and J. Y. Xiong, *J. Phys. Chem. B*, 2005, **109**, 24231.
11 X. Y. Liu and P. D. Sawant, *ChemPhysChem*, 2002, **4**, 374.
12 X. Y. Liu and P. D. Sawant, *Adv. Mater.*, 2002, **14**, 421.
13 X. Y. Liu and P. D. Sawant, *Appl. Phys. Lett.*, 2001, **79**, 3518.
14 J. L. Li, R. Y. Wang, X. Y. Liu and H. H. Pan, *J. Phys. Chem. B*, 2009, **113**, 5011.
15 M. A. Rogers and A. G. Marangoni, *Langmuir*, 2009, **25**, 5886.
16 M. A. Rogers and A. G. Marangoni, *Cryst. Growth Des.*, 2008, **8**, 4596.
17 P. Terech and R. G. Weiss, *Chem. Rev.*, 1997, **97**, 3133.
18 R. G. Weiss and P. Terech, *Molecular Gels Materials with Self-Assembled Fibrillar Networks*, Springer, Dordrecht, The Netherlands, 2007.
19 M. Suzuki, Y. Nakajima, M. Yumoto, M. Kimura, H. Shirai and K. Hanabusa, *Langmuir*, 2003, **19**, 8622.
20 R. Wang, X. Y. Liu, J. Xiong and J. J. Li, *J. Phys. Chem. B*, 2006, **110**, 7275.
21 X. Y. Liu, *Top. Curr. Chem.*, 2005, **256**, 1.
22 D. Lin-Vien, N. B. Colthup, W. G. Fateley and H. G. Grasselli, *The Handbook of Infrared and Raman Characteristic Frequencies of Organic Molecules*, Academic Press, NY, 1991.
23 A. G. Marangoni, Crystallization Kinetics, in *Fat CrystalNetworks*, ed. A. G. Marangoni, Marcel Dekker, New York, 2005, pp. 21–82.

